

# Energy-independent PWA of the reaction $\gamma p \rightarrow K^+ \Lambda$

A.V. Anisovich<sup>1,2</sup>, R. Beck<sup>1</sup>, V. Burkert<sup>3</sup>, E. Klempt<sup>1</sup>, M.E. McCracken<sup>4,5</sup>, V.A. Nikonov<sup>1,2</sup>, A.V. Sarantsev<sup>1,2</sup>, R.A. Schumacher<sup>5</sup>, U. Thoma<sup>1</sup>

<sup>1</sup> Helmholtz-Institut für Strahlen- und Kernphysik, Universität Bonn, Germany

<sup>2</sup> Petersburg Nuclear Physics Institute, Gatchina, Russia

<sup>3</sup> Jefferson Lab, 12000 Jefferson Avenue, Newport News, Virginia, USA

<sup>4</sup> Washington & Jefferson College, Washington, Pennsylvania, USA

<sup>5</sup> Carnegie Mellon University, 5000 Forbes Ave., Pittsburgh, Pennsylvania 15213, USA

Received: April 18, 2014/ Revised version:

**Abstract.** Using all recent data on the differential cross sections and spin observables for the reaction  $\gamma p \rightarrow K^+ \Lambda$ , an energy-independent partial-wave analysis is performed. The analysis requires multipoles up to  $L = 2$ ; there is no evidence that the fit requires multipoles with  $L = 3$ . At present the available data allow us to extract the dominant multipoles only. These are compatible with the multipoles obtained in the energy-dependent fit. This result supports the reliability of the Bonn-Gatchina energy-dependent results.

## 1 Introduction

The spectrum of excited nucleons ( $N^*$ ) reflects the structure of quantum chromodynamics in the non-perturbative regime. Full elucidation of the properties of the  $N^*$  states is an important long-term goal for the hadron physics community. The majority of experimental information has historically come from nucleon and pion-induced elastic and inelastic reaction channels. Partial-wave analyses of these data have established a rich spectrum of  $N^*$  states, so that the Particle Data Group [1] lists, for example, well-established (*i.e.*, “existence is certain” rating) nucleon resonances with spins up to  $9/2$ . In recent years, new experiments have produced high-precision measurements of photo-production of several hadronic final states due to the availability of high quality photon and electron beams at facilities including CLAS/Jefferson Lab, ELSA/Bonn, MAMI/Mainz, LEPS/SPring-8, and GRAAL/Grenoble. These have had a significant impact on our understanding of  $N^*$  properties. The present paper dwells on the production of a strangeness-containing final state. The reaction

$$\gamma p \rightarrow K^+ \Lambda \quad (1)$$

is sensitive to  $N^*$  states with masses in the range from 1.6 to 2.4 GeV, a two-body final state in a domain where pionic reactions are dominated by more complicated multi-pion final states. This makes it attractive to study, since the simple kinematics gives straightforward access to non-strange excitations in a mass range that is otherwise not well understood.

Theoretical work using a relativized constituent quark model made predictions about the spectrum of  $N^*$  and  $\Delta$  excitations [2, 3], as well as their couplings to various initial and final states including hyperonic [4] states. Many of the observed  $N^*$  resonances, as well as many “missing” resonances that have not

been observed coupling to  $\pi N$  were tabulated. One goal of  $N^*$  spectroscopy programs is thus to search for such missing states in channels other than  $\pi N$ .

All pseudo-scalar meson photoproduction reactions are characterized by eight complex amplitudes; parity invariance of the strong interaction reduces this number to four independent amplitudes. Full characterization of the reaction at a given kinematic relies upon measurement of  $d\sigma/d\Omega$  and at least seven of the fifteen single- and double-polarization observables [5]. However, for the sake of redundancy and the reduction of experimental ambiguities, as broad a range of observables as feasible must be analyzed for a full decomposition of a reaction at the amplitude level. In most theoretical or phenomenological studies, these amplitudes are constructed for each bin in energy and angle. In a next step, the set of amplitudes at a given energy can be expanded into multipoles which contain the information on the underlying physical processes.

Less demanding is to use only a finite number of multipoles in a truncated partial-wave expansion of the photoproduction amplitude. For small numbers of contributing partial waves, five observables can already be sufficient to determine the amplitudes [6, 7]. For example, seven observables have been measured for  $\gamma p \rightarrow \pi^0 p$ , the differential cross section  $d\sigma/d\Omega$ , the beam asymmetry  $\Sigma$ , target asymmetry  $T$ , the recoil polarization  $P$ , and different correlations between photon and target polarization yielding  $G$ ,  $E$ , and  $H$ . The seven data sets span a common mass range from 1.462 to 1.662 GeV in which no contributions with orbital angular momenta  $L \geq 3$  are expected. A truncated partial-wave analysis returned multipoles with  $L = 0, 1$  and  $2$  [8]. These multipoles lead to the excitation of nucleon and  $\Delta$  resonances. In the 1500 MeV region, however, the impact of  $\Delta$  resonances is small, and that is why the  $N(1520)3/2^-$  helicity coupling could be determined in [8].

The  $\gamma p \rightarrow K^+ \Lambda$  reaction profits from the fact that - due to isospin conservation - only isospin-1/2 intermediate states contribute and thus all  $\Delta$  excitations are excluded. Furthermore, the weak decay of the  $\Lambda$  to  $\pi N$  allows for determination of its recoil polarization. Use of polarized photon beams gives access to other polarization observables, notably the beam asymmetry ( $\Sigma$ ), and beam-recoil double-polarization observables for both circular ( $C_x$ ,  $C_z$ ) and linear ( $O_x$ ,  $O_z$ ) photon polarizations. Recent and forthcoming measurements from experiments with polarized nucleon targets will give access to the remaining set of polarization observables. For these reasons, the  $\gamma p \rightarrow K^+ \Lambda$  reaction is presently the best candidate for full amplitude-level characterization.

So far, all partial-wave analyses (PWA) of the reaction  $\gamma p \rightarrow K^+ \Lambda$  used energy-dependent representations of the contributing  $N^*$  states in the reaction. We shortly review these analyses in Sec. 2. Energy-dependent analyses benefit from the analytic structure of the amplitudes. However, the dominant partial waves over a range of energies could tend to mask the contributions of weaker partial waves nearby due to the force of statistics. A crucial test of the validity of this approach is to compare it to the results of an energy-independent analysis. The two approaches should agree within their respective limitations. Here we present application of the Bonn-Gatchina (BnGa) model to the  $\gamma p \rightarrow K^+ \Lambda$  reaction data in eleven independent energy bins from threshold up to  $\sqrt{s} = 1918$  MeV, as itemized in Sec. 3. The formalism is reviewed in Sec. 4. Results are discussed in Sec. 5, where we compare the fits with the latest energy-dependent BnGa multi-channel PWA. We also compare the energy-independent fits with multipolarity  $L = 0, 1$  with those including  $L = 2$  to assess the need for higher  $J^P$  intermediate states in the  $\gamma p \rightarrow K^+ \Lambda$  reaction. We show how using the energy-independent solution can be used to check the stability of earlier energy-dependent fit results. Sec. 6 summarizes our findings.

## 2 Energy-dependent analyses

In light of the several attractive features of the  $\gamma p \rightarrow K^+ \Lambda$  reaction, it has been the most suitable candidate for partial-wave analysis (PWA); several analyses have been performed with varied techniques and results. Early analyses [9] applied a single-channel tree-level resonant isobar model to SAPHIR  $d\sigma/d\Omega$  data [10] and found contributions from known  $N(1650)1/2^-$ ,  $N(1710)1/2^+$ , and  $N(1720)3/2^+$  states, as well as evidence for a previously unobserved  $3/2^-$  state with a mass of 1894 MeV. Soon after, other work showed features of the SAPHIR data that had been interpreted as resonant contributions could be described in a Regge model [11] to describe  $t$ -channel exchange of strange mesons [12]. The group at Ghent [13] used the Regge-plus-resonance approach to analyze forward-angle  $d\sigma/d\Omega$  and  $P$  data and found evidence for  $N(1650)1/2^-$ ,  $N(1710)1/2^+$ , and  $N(1720)3/2^+$  states near threshold and  $J^P = 3/2^+$  and  $1/2^+$  states with masses near 1.9 GeV. Exploratory PWA studies at  $\sqrt{s} > 2.0$  GeV indicate resonance structure near 2.1 GeV, for example in [14], but in the present study we only work with multipoles below about 1.92 GeV.

Interpretation of  $K^+ \Lambda$  production mechanism was complicated when  $d\sigma/d\Omega$  and recoil polarization data published

by the CLAS Collaboration [15, 16] showed significant differences when compared to the SAPHIR data. The implications were studied and discussed by Mart *et al.* [17] and others in both single-channel effective Lagrangian models and multipole analyses.

The Bonn-Gatchina Group produced several PWA studies over the years of the  $\gamma p \rightarrow K^+ \Lambda$  reaction. A 2005 publication Sarantsev *et al.* [18] demonstrated that partial-wave analysis of  $d\sigma/d\Omega$ ,  $\Sigma$  and  $P$  data, when coupled with data from photoproduction of  $K\Sigma$ ,  $\pi N$ , and  $\eta N$ , necessitates a  $J^P = 1/2^+$  state with mass of approximately 1840 MeV. It also suggested the existence of four  $3/2^-$  states between 1520 and 2170 MeV, but produces no evidence for  $1/2^-$  states of mass above 1650 MeV. They noted that the discrepancy between the then available SAPHIR and CLAS  $d\sigma/d\Omega$  results could lead to ambiguities in fitting. With the publication [19], Anisovich *et al.* incorporated the large spin-transfer probability observables  $C_x$  and  $C_z$  measured with circularly polarized photons at CLAS [20] into an analysis coupling several observables from  $\pi$ ,  $\eta$ , and  $K$  photoproduction reactions. This analysis showed that all observables could be reproduced with the further addition of only one state, a  $3/2^+$  resonance with mass of approximately 1900 MeV. The 2010 publication of higher-statistics and independent results from CLAS [21], the discrepancy in the cross section for  $\gamma p \rightarrow K^+ \Lambda$  seems to have been resolved. Reduced ambiguity in PWA of the channel was thus expected.

The most recent BnGa analyses have applied coupled-channel PWA to a large set of observables for many reactions [22], and extracted transition amplitudes for pion- and photon-induced production of  $\eta$  and  $K$  mesons [23]. These analyses show that adequate description of the data is possible with two separate sets of resonances, distinguished by the presence of either one or two  $7/2^+$  states. A subsequent multi-channel analysis [24] focusing on information from  $K\Sigma^0$  production, provided an updated set of resonance contributions (referred to here as BnGa2013), but concluded that further polarization information for  $\Sigma^0$  production is needed to unambiguously determine production amplitudes for these reactions.

## 3 Data on $\gamma p \rightarrow K^+ \Lambda$

In the region from threshold up to  $\sqrt{s} = 1918$  MeV the following data are used: differential cross section  $d\sigma/d\Omega$  from [15] and [21], recoil polarization  $P$  from [21] and [25],  $\Sigma$  from [25],  $T$ ,  $O_x$  and  $O_z$  from [26], and the spin transfer coefficients  $C_x$  and  $C_z$  from [20]. In the low energy bin the recent data on  $d\sigma/d\Omega$  from CB@MAMI [27] are also used. The fitting region was divided into eleven energy bins in  $\sqrt{s}$  each containing data on at least one double polarization observable: 1642 – 1653, 1672 – 1683, 1697 – 1708, 1727 – 1738, 1752 – 1758, 1777 – 1788, 1807 – 1818, 1832 – 1843, 1857 – 1868, 1882 – 1893, 1900 – 1918 (in MeV). The data are shown in Fig. 1 jointly with the BnGa2013 energy-dependent fit and two further fits described below. The data are organized in eleven blocks each containing the eight observables.

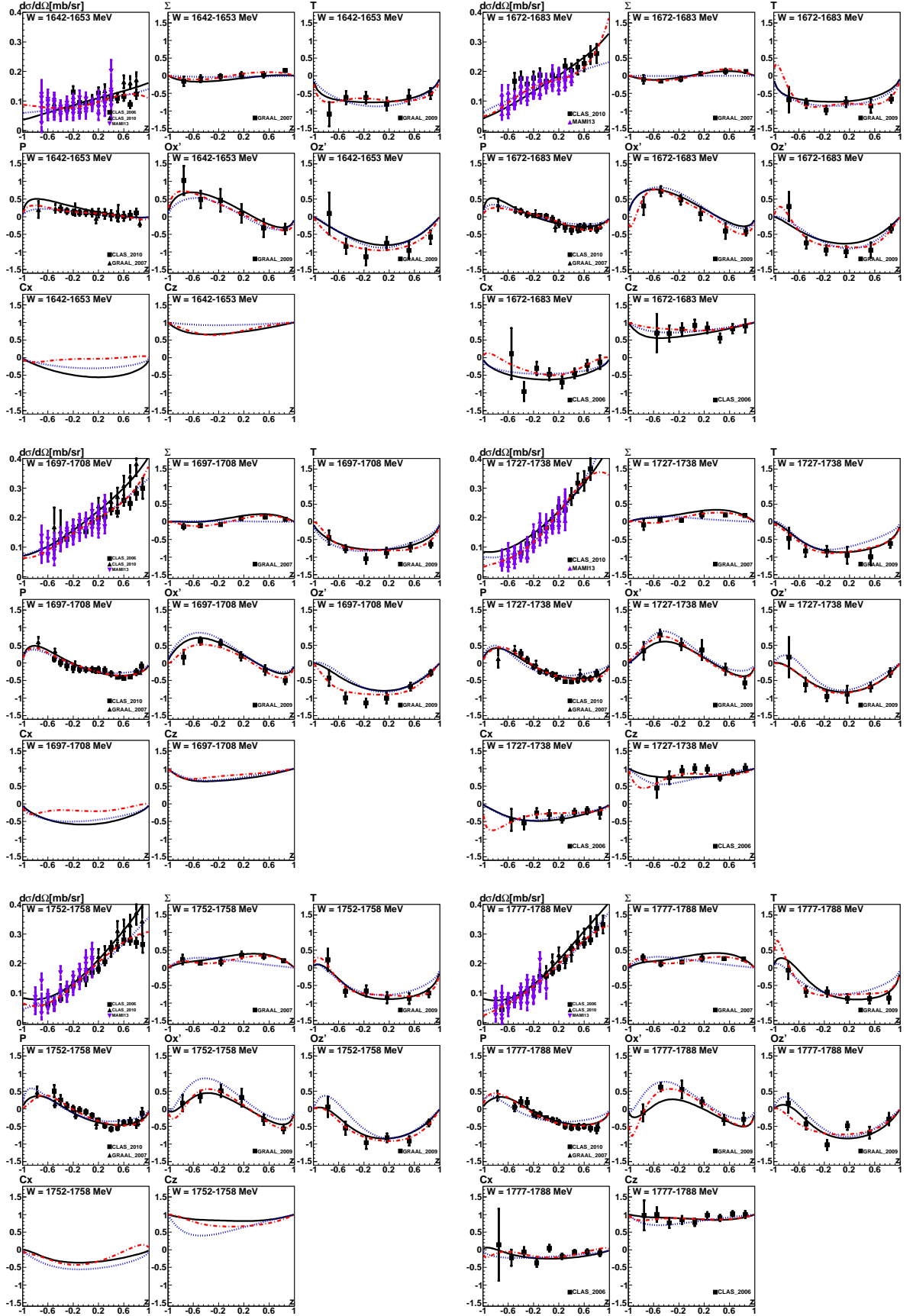


**Fig. 1.** Data and fit to data on  $\gamma p \rightarrow K^+ \Lambda$ . Black line is the energy-dependent solution BnGa2013, the dashed (blue) line is the truncated PWA with  $L = 0, 1$ , and dot-dashed (red) line the truncated PWA with  $L = 0, 1, 2$ .



## 4 Formalism

The amplitude for photoproduction of a single pseudoscalar meson is well known and can be found in the literature (see for example [28] and references therein). Here, we consider the case of a  $K^+$  meson recoiling against a  $\Lambda$  hyperon. The general structure of the amplitude can be written in the form

$$A = \omega^* J_\mu \varepsilon_\mu \omega',$$

where  $\omega'$  and  $\omega$  are spinors representing the baryon in the initial and final state,  $J_\mu$  is the electromagnetic current of the electron, and  $\varepsilon_\mu$  characterizes the polarization of the photon. The full amplitude can be expanded into four invariant (CGLN) amplitudes  $\mathcal{F}_i$  [5]

$$J_\mu = i\mathcal{F}_1 \sigma_\mu + \mathcal{F}_2 (\boldsymbol{\sigma} \mathbf{q}) \frac{\varepsilon_{\mu ij} \sigma_i k_j}{|\mathbf{k}| |\mathbf{q}|} + i\mathcal{F}_3 \frac{(\boldsymbol{\sigma} \mathbf{k})}{|\mathbf{k}| |\mathbf{q}|} q_\mu + i\mathcal{F}_4 \frac{(\boldsymbol{\sigma} \mathbf{q})}{q^2} q_\mu. \quad (2)$$

where  $\mathbf{q}$  is the momentum of the nucleon in the  $K^+ \Lambda$  channel,  $\mathbf{k}$  is the momentum of the nucleon in the  $\gamma N$  channel calculated in the center-of-mass system of the reaction, and  $\sigma_i$  are the Pauli matrices.

The functions  $\mathcal{F}_i$  have the following angular dependence:

$$\begin{aligned} \mathcal{F}_1(W, z) &= \sum_{L=0}^{\infty} [LM_{L+} + E_{L+}] P'_{L+1}(z) + \\ &\quad [(L+1)M_{L-} + E_{L-}] P'_{L-1}(z), \\ \mathcal{F}_2(W, z) &= \sum_{L=1}^{\infty} [(L+1)M_{L+} + LM_{L-}] P'_L(z), \\ \mathcal{F}_3(W, z) &= \sum_{L=1}^{\infty} [E_{L+} - M_{L+}] P''_{L+1}(z) + \\ &\quad [E_{L-} + M_{L-}] P''_{L-1}(z), \\ \mathcal{F}_4(W, z) &= \sum_{L=2}^{\infty} [M_{L+} - E_{L+} - M_{L-} - E_{L-}] P''_L(z). \end{aligned} \quad (3)$$

Here,  $L$  corresponds to the orbital angular momentum in the  $K^+ \Lambda$  system,  $W$  is the total energy,  $P_L(z)$  are Legendre polynomials with  $z = (\mathbf{k} \mathbf{q}) / (|\mathbf{k}| |\mathbf{q}|)$ , and  $E_{L\pm}$  and  $M_{L\pm}$  are electric and magnetic multipoles describing transitions to states with  $J = L \pm 1/2$ . There are no contributions from  $M_{0+}$ ,  $E_{0-}$ , and  $E_{1-}$  for spin 1/2 resonances.

Differential cross section and polarization observables can be expressed in terms of the  $\mathcal{F}_i$  functions. The relations can be found, e.g., in [29]. For convenience, we give the expressions for the observables used in the fit. The single polarization observables  $\Sigma$ ,  $P$  and  $T$  are given by

$$\Sigma I = -\frac{\sin^2(\theta)}{2} \quad (4)$$

$$P I = \sin(\theta) \text{Im}[(2\mathcal{F}_2^* + \mathcal{F}_3^* + z\mathcal{F}_4^*)\mathcal{F}_1 + \mathcal{F}_2^*(z\mathcal{F}_3 + \mathcal{F}_4) + \sin^2(\theta)\mathcal{F}_3^*\mathcal{F}_4], \quad (5)$$

$$T I = \sin(\theta) \text{Im}[\mathcal{F}_1^*\mathcal{F}_3 - \mathcal{F}_2^*\mathcal{F}_4 + z(\mathcal{F}_1^*\mathcal{F}_4 - \mathcal{F}_2^*\mathcal{F}_3) - \sin^2(\theta)\mathcal{F}_3^*\mathcal{F}_4], \quad (6)$$

where

$$I = \text{Re}[\mathcal{F}_1\mathcal{F}_1^* + \mathcal{F}_2\mathcal{F}_2^* - 2z\mathcal{F}_2\mathcal{F}_1^* + \frac{\sin^2(\theta)}{2}(\mathcal{F}_3\mathcal{F}_3^* + \mathcal{F}_4\mathcal{F}_4^* + 2\mathcal{F}_4\mathcal{F}_1^* + 2\mathcal{F}_3\mathcal{F}_2^* + 2z\mathcal{F}_4\mathcal{F}_3^*)]. \quad (7)$$

Here the center of mass (c.m.) scattering angle is  $\theta$ . The double polarization observables  $O_{x'}$ ,  $O_{z'}$ ,  $C_x$  and  $C_z$  can be written as

$$O_{x'} I = \sin(\theta) \text{Im}[\mathcal{F}_2\mathcal{F}_3^* - \mathcal{F}_1\mathcal{F}_4^* + z(\mathcal{F}_2\mathcal{F}_4^* - \mathcal{F}_1\mathcal{F}_3^*)], \quad (8)$$

$$O_{z'} I = -\sin^2(\theta) \text{Im}[\mathcal{F}_1\mathcal{F}_3^* + \mathcal{F}_2\mathcal{F}_4^*], \quad (9)$$

$$C_x = \sin(\theta)C_{z'} + \cos(\theta)C_{x'}, \quad (10)$$

$$C_z = \cos(\theta)C_{z'} - \sin(\theta)C_{x'}, \quad (11)$$

where

$$C_{x'} I = \sin(\theta) \text{Re}[\mathcal{F}_2\mathcal{F}_2^* - \mathcal{F}_1\mathcal{F}_1^* + \mathcal{F}_2\mathcal{F}_3^* - \mathcal{F}_1\mathcal{F}_4^* + z(\mathcal{F}_2\mathcal{F}_4^* - \mathcal{F}_1\mathcal{F}_3^*)], \quad (12)$$

$$C_{z'} I = \text{Re}[-2\mathcal{F}_1\mathcal{F}_2^* + z(\mathcal{F}_1\mathcal{F}_1^* + \mathcal{F}_2\mathcal{F}_2^*) - \sin^2(\theta)(\mathcal{F}_1\mathcal{F}_3^* + \mathcal{F}_2\mathcal{F}_4^*)]. \quad (13)$$

Let us remind the reader that the  $z$  axis defines the direction of the incoming particles in the c.m. system, while the  $z'$  axis defines the direction of the outgoing particles (see [29]). Finally the differential cross section is equal to:

$$\frac{d\sigma}{d\Omega} = \frac{k}{q} I, \quad (14)$$

where  $q$  and  $k$  are the moduli of the initial and final c.m. momenta, respectively.

## 5 Energy-independent truncated PWA

The energy-independent (or single energy) PWA uses the full database of the Bonn-Gatchina partial-wave analysis [22]. A reasonable description of all data is achieved; the breakdown of the  $\chi^2$  contribution from various data sets is given in Table 1. In the following, we use the data on the reaction  $\gamma p \rightarrow K^+ \Lambda$  only.

### 5.1 Energy-independent PWA with $L = 0, 1$ multipoles

It is natural to assume that in the energy region not far above the threshold only multipoles of low spin play a role. The energy dependent PWA [23] supports this assumption: in the region up to 2000 MeV there are four large multipoles,  $E_{0+}$ ,  $E_{1+}$ ,  $M_{1+}$  and  $M_{1-}$  which are 5 to 10 times larger than multipoles with  $L = 2$ .

The multipole decomposition is shown in Fig. 2. In the fit, it is assumed that only the four multipoles shown in the figure contribute to the reaction  $\gamma p \rightarrow K^+ \Lambda$ , all other contributions are set to zero. The errors of the multipoles correspond to changes in description of the data by one unit in of  $\chi^2$ . Let us note that the phases of the multipoles in a fit are defined up to



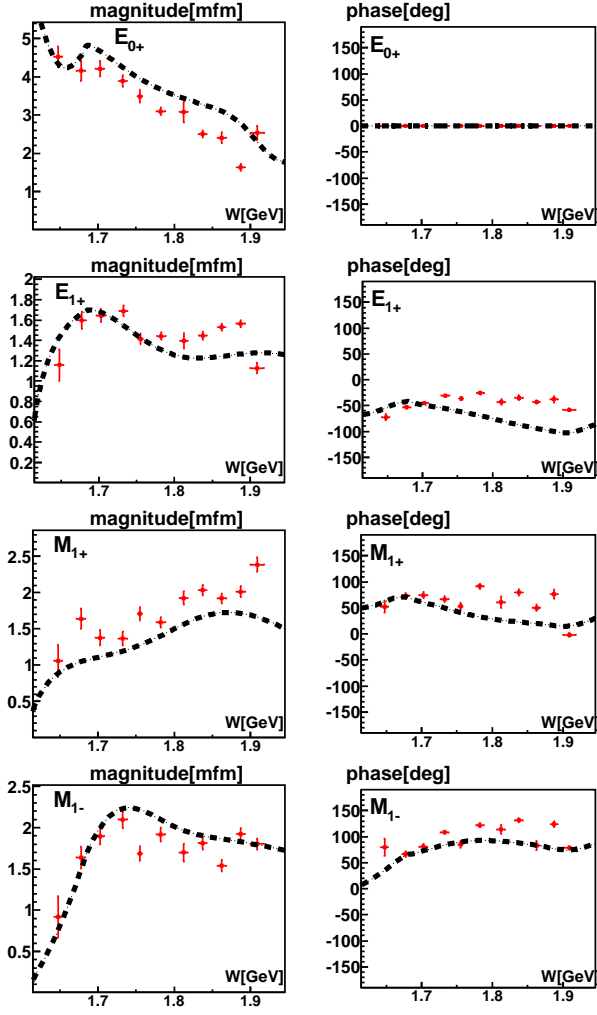


**Fig. 2.** Decomposition of the  $\gamma p \rightarrow K^+ \Lambda$  amplitude with  $S$  and  $P$  multipoles. The general phase is not defined so we choose  $\phi(E_0^+) = 0$ . The dashed line is the energy dependent solution BnGa2013.

one overall phase. Here, we determine the phases relative to the phase of the  $E_{0+}$  multipole. Hence  $\phi(E_0^+) = 0$  holds by construction. The comparison with the Bonn-Gatchina PWA shows that the energy-dependent fit is approximately compatible with the single-energy fit, at least in the region up to 1750 MeV. We also note that a truncated PWA with  $L = 0, 1$  multipoles gives a good description of the data up to this energy. At  $W > 1800$  MeV the  $L = 2$  multipoles are important, see Fig. 1. The quality of this fit (in terms of  $\chi^2$ ) is shown in Table 1. While the differential cross sections are described very reasonably, the fit to polarization observables is not convincing: in particular the beam asymmetry is poorly reproduced and several other polarization variables have  $\chi^2$  values exceeding 2. A more detailed view reveals that the predicted beam asymmetry  $\Sigma$  and the data have a different angular dependence; this difference is rather pronounced in the mass region above 1800 MeV. Obviously, a fit with only  $L = 0$  and  $L = 1$  multipoles is not sufficient to describe the data over the full mass range.

## 5.2 Energy-independent PWA with $L = 0, 1, 2$ multipoles

The multipoles with  $L = 2$  significantly improve the fit quality. The mean  $\chi^2$  per data point drops from 1.8 to 0.8 (see Table 1). The improvement is particularly large for the GRAAL beam asymmetry where the  $\chi^2$  goes down from 6.77 to 0.57. Most observables are now fitted with a  $\chi^2$  per data point of less than 1. The number of fit parameters (moduli of 8 amplitudes and 7 phases at 11 energies) is 165. It is likely that the systematic errors given in the publications are slightly overestimated. The improvement of the fit can also be seen when Fig. 1 is inspected.

The resulting multipole decomposition is shown in the two left columns of Fig. 3. We observe that the multipoles scatter from bin to bin. Moreover, for some energy bins there are no  $C_x$  and  $C_z$  data. The solution is no longer uniquely defined: two different solutions are found which differ less than  $\delta\chi^2 < 1$ . Two conclusions follow from these observations: i) at energies  $W > 1750$  MeV the  $L = 2$  multipoles are definitely needed. ii) the lack of experimental data and the data quality does not allow extraction of multipoles with the desired precision in a completely free fit.

## 5.3 Energy-independent PWA with $L = 0, 1, 2$ multipoles and penalty function

In a next step we guide the fit with  $L = 0, 1, 2$  multipoles so it is not totally free. We assume that the large multipoles with  $L = 0, 1$  are reasonably well defined by the fit using  $L = 0, 1$  multipoles only. Thus we impose a penalty function which sanctions solutions which deviate strongly from the fit with  $L = 0, 1$  multipoles. More precisely, we introduce a penalty function defined as

$$\chi_{pen}^2 = \sum_{\alpha} \frac{(M_{\alpha} - M_{\alpha}^{0,1})^2}{(\delta M_{\alpha}^{0,1})^2} + \sum_{\alpha} \frac{(E_{\alpha} - E_{\alpha}^{0,1})^2}{(\delta E_{\alpha}^{0,1})^2}, \quad (15)$$

where  $E_{\alpha}^{0,1}$  and  $M_{\alpha}^{0,1}$  are the electric and magnetic multipoles from solution with  $L = 0, 1$  multipoles only;  $\delta E_{\alpha}^{0,1}$ ,  $\delta M_{\alpha}^{0,1}$  are the multipole uncertainties.

The quality of the fit to the differential cross sections hardly changes while most polarization observables are now described with lesser accuracy (see Table 1).

The resulting multipoles are shown in the two center columns of Fig. 3. There is now a unique solution but the solution still scatters significantly for the small multipoles, and the  $E_{0+}$  and  $M_{1+}$  waves deviate significantly from the energy-dependent fit. It has to be stressed that so far, the solution has no bias at all; the solution is constructed from the experimental data without any input from the energy-dependent solution. Even though there are discrepancies between the energy-dependent and independent solution in detail, the overall agreement is very satisfactory. In particular there is no hint that an additional narrow resonance may be hidden or that too many resonances have been used to fit the data.

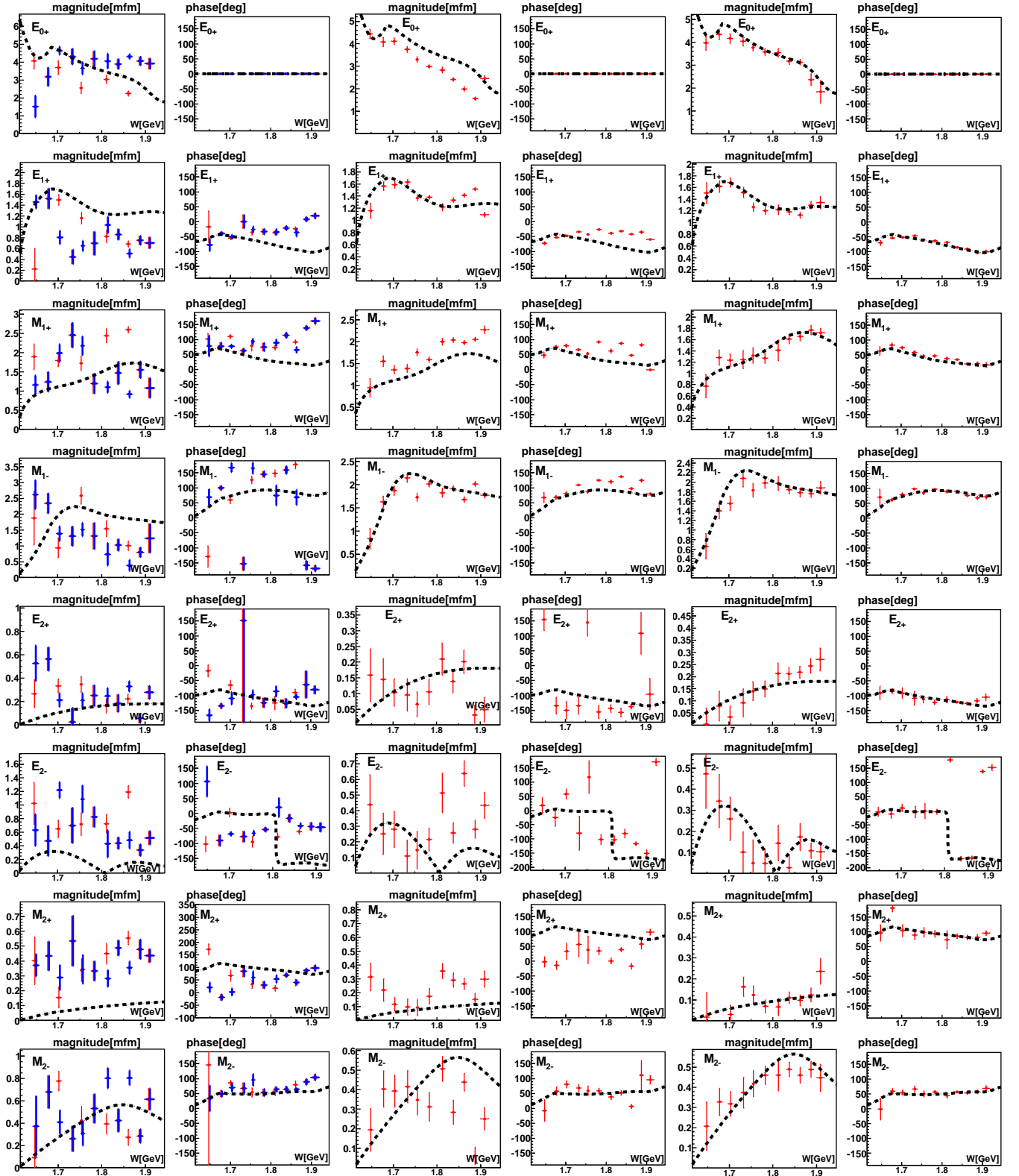


Fig. 3. Decomposition of the  $\gamma p \rightarrow K^+ \Lambda$  amplitude with  $S$ ,  $P$ , and  $D$  multipoles. In the low-energy region, two solutions (red and blue) exist which give identical fits to the data. The dashed line is the energy-dependent solution BnGa2013. The left two columns represent a free fit. In the two center columns, the penalty function (Eq. 15) is used. For the two columns on the right, (Eq. 16) is used.

**Table 1.** Quality of the energy-independent fit:  $\chi^2/N_{\text{data}}$  and number of data points (in brackets).

Data	BnGa 2013	EI PWA $L = 0, 1$	EI PWA $L = 0, 1, 2$	EI PWA penalty	BnGa2013 penalty
$d\sigma/d\Omega$ (CLAS+GRAAL)	1.85 (316)	1.15	0.81	0.82	0.85
$d\sigma/d\Omega$ (MAMI)	1.55 (510)	1.05	0.84	0.87	0.87
$\Sigma$ (GRAAL)	2.44 (66)	6.77	0.57	2.08	0.81
$P$ (CLAS)	1.2 (184)	3.02	0.80	1.03	0.86
$P$ (GRAAL)	0.65 (66)	2.49	0.68	1.27	0.64
$T$	1.54 (66)	2.02	0.61	1.20	0.98
$O_{x'}$	1.73 (66)	3.29	0.42	1.53	1.24
$O_{z'}$	1.88 (66)	2.68	0.81	1.13	1.19
$C_x$	1.64 (43)	1.10	0.99	1.17	1.01
$C_z$	1.65 (43)	1.94	1.39	2.49	1.36
Mean	1.57	1.8	0.8	0.9	0.85

#### 5.4 Constrained energy-independent PWA as a test of the energy dependent solution

The energy-independent solution can be used as a test of the energy-dependent solution BnGa2013 PWA [23]. The goals are to check the stability of energy-dependent multipoles  $L = 0, 1, 2$  and to search for any missing structures. Thus the penalty function, Eq. 16, is included in the fit to control the deviation of  $L = 0, 1, 2$  multipoles from the BnGa2013 solution:

$$\chi_{\text{pen}}^2 = \sum_{\alpha} \frac{(M_{\alpha} - M_{\alpha}^{0,1,2})^2}{(\delta M_{\alpha}^{0,1,2})^2} + \sum_{\alpha} \frac{(E_{\alpha} - E_{\alpha}^{0,1,2})^2}{(\delta E_{\alpha}^{0,1,2})^2}, \quad (16)$$

where  $E_{\alpha}^{0,1,2}$  and  $M_{\alpha}^{0,1,2}$  are the multipoles for BnGa2013  $L = 0, 1, 2$  solution and  $\delta E_{\alpha}^{0,1,2}$ ,  $\delta M_{\alpha}^{0,1,2}$  are the multipole uncertainties for the fit without penalty. In this approach, multipoles with  $L \geq 3$  are fixed by the energy-dependent solution. The error in the multipoles from the BnGa2013 energy-dependent solution is not included in the definition of the penalty function. The result of the fit is shown in the two columns on the right in Fig. 3.

The fit is only marginally worse than the unconstrained fit. This proves the quality of the energy-dependent fit.

## 6 Conclusion

We have performed an energy-independent partial-wave analysis for the reaction  $\gamma p \rightarrow K^+ \Lambda$  in the region up to an invariant mass  $W = 1918$  MeV. Although not yet complete, a data set of differential cross section values and polarization observables was available that allowed an energy-independent extraction of the dominant electromagnetic multipoles that underlie the production process. The analysis requires multipoles up to  $L = 2$ , and there is no evidence that the fit requires multipoles with  $L \geq 3$ .

At present the available data allow for the extraction of multipoles  $E_{0+}$ ,  $E_{1+}$ ,  $M_{1+}$  and  $M_{1-}$  only, without using further constraints. They are compatible with multipoles obtained in the energy-dependent fit. Multipoles with  $L = 2$  could not be extracted unambiguously without imposing further, albeit rather mild constraints.

The multipoles from the energy-dependent PWA BnGa2013 were checked for stability in the single-energy fit constrained by BnGa2013 solution. The resulting multipoles are very close to the original energy-dependent solution. There is no evidence for any additional structures which may have escaped in the energy-dependent fit.

These results demonstrate that using cross section and polarization observables for the photoproduction of pseudoscalar mesons can be successfully employed in energy-independent PWA without additional constraints, and that the complex multipoles underlying the production process can be determined with good accuracy. It is also demonstrated that the multipoles determined in this manner are consistent with those determined in more strongly constrained energy-dependent PWA fits.

These results mark an essential step in the ongoing development of sound procedures in the search for yet-to-be discovered excited states of the nucleon. Using data from major single production channels only, the method enables an independent verification of discovery claims of new excited states in complex and highly constrained coupled-channel analyses.

## References

1. J. Beringer et al. (Particle Data Group), Phys. Rev. D **86**, 010001 (2012)
2. S. Capstick and W. Roberts, Phys. Rev. D **47**, 1994-2010 (1993).
3. S. Capstick and W. Roberts, Phys. Rev. D **57**, 4301 (1998).
4. S. Capstick and W. Roberts, Phys. Rev. D **58**, 074011 (1998).
5. W.-T. Chiang and F. Tabakin, Phys. Rev. C **55**, 2054 (1997).
6. A.S. Omelaenko, Sov.J.Nucl.Phys. **34**, 406 (1981).
7. Y. Wunderlich, R. Beck and L. Tiator, "Ambiguities of the single spin observables in a truncated partial wave expansion for photoproduction of pseudoscalar mesons," arXiv:1312.0245 [nucl-th].
8. Jan Hartmann *et al.* [CBELSA/TAPS collaboration], "The  $N(1520)$  helicity amplitude from an energy-independent multipole analysis based on new polarization data", submitted to Phys. Rev. Lett. (2014).
9. T. Mart and C. Bennhold, Phys. Rev. C **61**, 012201 (1999).
10. K. H. Glander *et al.* [SAPHIR Collaboration], Eur. Phys. J. A **19**, 251 (2004).
11. M. Guidal, J.-M. Laget, and M. Vanderhaeghen, Phys. Rev. C **68**, 058201 (2003).



12. S. Janssen, J. Ryckebusch, D. Debruyne, and T. Van Cauteren, Phys. Rev. C **65**, 015201 (2001).
13. T. Corthals, J. Ryckebusch, and T. Van Cauteren, Phys. Rev. C **73**, 045207 (2006).
14. R. A. Schumacher and M. M. Sargsian, Phys. Rev. C **83**, 025207 (2011).
15. R. Bradford *et al.* [CLAS Collaboration], Phys. Rev. C **73**, 035202 (2006).
16. J. W. C. McNabb *et al.* [CLAS Collaboration], Phys. Rev. C **69**, 042201 (2004).
17. T. Mart and A. Sulaksono, and references therein, Phys. Rev. C **74**, 055203 (2006).
18. A.V. Sarantsev, V.A. Nikonov, A.V. Anisovich, E. Klempt, U. Thoma, Eur. Phys. J. A **25**, 3 (2005).
19. A.V. Anisovich, V. Kleber, E. Klempt, V.A. Nikonov, A.V. Sarantsev, U. Thoma, Eur. Phys. J. A **34**, 243 (2007).
20. R. Bradford *et al.* [CLAS Collaboration], Phys. Rev. C **75**, 035205 (2007).
21. M. E. McCracken *et al.* [CLAS Collaboration], Phys. Rev. C **81**, 025201 (2010).
22. A. V. Anisovich, R. Beck, E. Klempt, V. A. Nikonov, A. V. Sarantsev and U. Thoma, Eur. Phys. J. A **48**, 15 (2012).
23. A. V. Anisovich, R. Beck, E. Klempt, V. A. Nikonov, A. V. Sarantsev and U. Thoma, Eur. Phys. J. A **48**, 88 (2012).
24. A. V. Anisovich, E. Klempt, V. A. Nikonov, A. V. Sarantsev and U. Thoma, Eur. Phys. J. A **49**, 158 (2013).
25. A. Lleres *et al.* [GRAAL Collaboration], Eur. Phys. J. A **31**, 79 (2007).
26. A. Lleres *et al.* [GRAAL Collaboration], Eur. Phys. J. A **39**, 149 (2009).
27. T. C. Jude *et al.* [Crystal Ball Collaboration], “ $K^+ \Lambda$  and  $K^+ \Sigma^0$  photoproduction with fine center-of-mass energy resolution,” arXiv:1308.5659 [nucl-ex].
28. D. Drechsel, O. Hanstein, S. S. Kamalov and L. Tiator, Nucl. Phys. A **645**, 145 (1999).
29. C. G. Fasano, F. Tabakin and B. Saghai, Phys. Rev. C **46**, 2430 (1992).